Published OnlineFirst August 3, 2016; DOI: 10.1158/0008-5472.CAN-15-3453

Tumor and Stem Cell Biology

Cancer Research

Inducing Differentiation of Premalignant Hepatic Cells as a Novel Therapeutic Strategy in Hepatocarcinoma

Benita Wolf[1], Kathrin Krieg[2], Christine Falk[3], Kai Breuhahn[4], Hildegard Keppeler[1], Tilo Biedermann[5,6], Evi Schmid[7], Steven Warmann[7], Joerg Fuchs[7], Silvia Vetter[8], Dennis Thiele[9], Maike Nieser[9], Meltem Avci-Adali[10], Yulia Skokowa[11], Ludger Schöls[12,13], Stefan Hauser[12], Marc Ringelhan[14,15,16], Tetyana Yevsa[17], Mathias Heikenwalder[15,16], and Uta Kossatz-Boehlert[1,2]

Abstract

Hepatocellular carcinoma (HCC) represents the second leading cause of cancer-related deaths and is reported to be resistant to chemotherapy caused by tumor-initiating cells. These tumor-initiating cells express stem cell markers. An accumulation of tumor-initiating cells can be found in 2% to 50% of all HCC and is correlated with a poor prognosis. Mechanisms that mediate chemoresistance include drug export, increased metabolism, and quiescence. Importantly, the mechanisms that regulate quiescence in tumor-initiating cells have not been analyzed in detail so far. In this research we have developed a single cell tracking method to follow up the fate of tumor-initiating cells during chemotherapy. Thereby, we were able to demonstrate that mCXCL1 exerts cellular state-specific effects regulating the resistance to chemotherapeutics. mCXCL1 is the mouse homolog of the human IL8, a chemokine that correlates with poor prognosis in HCC patients. We found that mCXCL1 blocks differentiation of premalignant cells and activates quiescence in tumor-initiating cells. This process depends on the activation of the mTORC1 kinase. Blocking of the mTORC1 kinase induces differentiation of tumor-initiating cells and allows their subsequent depletion using the chemotherapeutic drug doxorubicin. Our work deciphers the mCXCL1–mTORC1 pathway as crucial in liver cancer stem cell maintenance and highlights it as a novel target in combination with conventional chemotherapy. *Cancer Res; 76(18); 5550–61. ©2016 AACR.*

Introduction

Hepatocellular carcinoma (HCC) is resistant to chemotherapeutic regimens and is the second leading cause of cancer-associated deaths worldwide (1). In 28% to 50% of all HCC markers of hepatic progenitors and tumor-initiating cells (TIC) are expressed. Although their origin is still under debate, targeting TICs represents a promising therapeutic approach.

In this work, we took advantage of the characterized Cullin3 (Cul3) and Cul3/p53 knockout (ko) mouse model, in which loss of Cul3 leads to massive expansion of hepatic progenitors. Importantly, loss of Cul3 expression was detected in a large series of human liver cancers and correlated with tumor de-differentiation (2).

Cul3 is a multiprotein ubiquitin ligase, which controls the degradation of several proteins, including cyclin E (3). *In vivo*, hepatic Cul3 ko progenitors accumulate cyclin E and subsequent DNA damage, which triggers the p53 dependent activation of the senescence checkpoint to block transformation. Simultaneous

[1]Department of Internal Medicine I, University Hospital Tuebingen, Tuebingen, Germany. [2]Department for Clinical Pharmacology, University Hospital Tuebingen, Tuebingen, Germany. [3]Institute of Transplant Immunology, IFB-Tx, Hannover Medical School, Hannover, Germany. [4]Institute of Pathology, University Hospital Heidelberg, Heidelberg, Germany. [5]FACS Core Facility of the Interdisciplinary Center for Clinical Research of the University Hospital of Tuebingen, University of Tuebingen, Tuebingen, Germany. [6]Department of Dermatology and Allergy Biederstein, Technical University Munich, Munich, Germany. [7]Department of Pediatric Surgery and Pediatric Urology, University Hospital Tuebingen, Tuebingen, Germany. [8]Institute for Experimental and Clinical Pharmacology and Toxicology, University of Tuebingen, Tuebingen, Germany. [9]Institute of Pathology and Neuropathology, University Hospital of Tuebingen, Tuebingen, Germany. [10]Department of Thoracic and Cardiovascular Surgery, University Hospital Tuebingen, Tuebingen, Germany. [11]Division of Translational Oncology, Department of Hematology, Immunology, University Hospital Tuebingen. [12]German Center for Neurodegenerative Diseases (DZNE), Tuebingen, Germany. [13]Department of Neurology and Hertie-Institute for Clinical Brain Research, University of Tuebingen, Tuebingen, Germany. [14]Second Medical Department, Klinikum rechts der Isar, Technical University of Munich, Munich, Germany. [15]Division of Chronic Inflammation and Cancer, German Cancer Research Center (DKFZ), Heidelberg, Germany. [16]Institute of Virology, Technische Universität München (TUM)/Helmholtz Zentrum München (HMGU), Munich, Germany. [17]Department of Gastroenterology, Hepatology and Endocrinology, Hannover Medical School, Hannover, Germany.

Note: Supplementary data for this article are available at Cancer Research Online (http://cancerres.aacrjournals.org/).

B. Wolf and K. Krieg contributed equally to this article.

Current address for M. Heikenwalder: DKFZ, Heidelberg, Germany

Corresponding Author: Uta Kossatz-Boehlert, University Hospital Tuebingen, Auf der Morgenstelle 8, 72076 Tuebingen, Germany. Phone: 707-1297-4924; Fax: 707-129-5035; E-mail: uta.kossatz-boehlert@med.uni-tuebingen.de

doi: 10.1158/0008-5472.CAN-15-3453

loss of p53 and Cul3 causes transformation of the differentiating hepatic progenitors into TICs (2).

Based on the accumulation of DNA damage Cul3/p53 ko cells differentiate into premalignant cells and into TICs. Premalignant Cul3/p53 ko cells are $CD34^+$ and express the liver progenitor marker alpha-1-fetoprotein (AFP). Cells that differentiate downregulate CD34 accumulate DNA damage and are transformed into TICs upon loss of p53. Thus, TICs are $CD34^-$ express hepatic stem cell markers and tumor-initiating markers such as CD133 and CK19 (2, 4, 5). Cells isolated from livers of Cul3 ko and Cul3/p53 ko mouse models mimic the described *in vivo* phenotype (2). We, therefore, used these cells to identify differences in signaling pathways regulated by chemokines.

Materials and Methods

Cell lines

Cul3 ko and Cul3/p53 ko cells were described previously (2). HepT1 and Huh6 were provided by J.F. HepG2 and Huh7 cells were obtained from ATCC.

Authentication: HuH-7; JCRB 0403, HEP-G2; DSMZ ACC 180. HepT1, Huh6 were identified by their morphology and marker expression. All cell lines were treated with BM Cyclin (Roche) and tested for mycoplasma using DAPI and nested PCR.

In vitro treatment with Rad001, doxorubicin, mCXCL1/hCXCL8

Cells were seeded at a density of 2.5×10^5 cells per 6 cm plate and treated for 48 to 72 hours. Concentrations of all used chemicals were determined by titration and were as follows: 2 μg/mL doxorubicin, 7.5 μmol/L Rad001 (Novartis AG), and 0.013041 pg/cell/mL mCXCL1 (based on Luminex-analysis; Tocris) for Cul3/p53 ko. For hHCC cells, concentrations were as follows: doxorubicin 2 μg/mL, 7.5 μmol/L Rad001 (Novartis AG), and 0.015 pg/cell/mL of hCXCL8 (Tocris). After doxorubicin treatment prior to harvesting, cells were washed twice with PBS to remove free doxorubicin and dead cells. Cells were trypsinized, collected in 0.1% FCS/PBS, and used for analysis.

Differentiation stain

Cells were seeded at a density of 3.4×10^4 cells/well on coverslips [12-well plate (BD Transduction Lab), coated with 0.1% gelatin]. Fourteen-hour after incubation with mCXCL1 and Rad001, cells were stained for CD34 (BioLegend, 1:100). After incubation for 30 minutes, cells were washed and an anti-rat Alexa Fluor 555 (Invitrogen, dilution 1:200) antibody was used to detect $CD34^+$ cells. Cells were re-incubated in the appropriate medium for 8.5 hours and stained for CD34 receptor, which was detected using an anti-rat-FITC antibody (Dianova, dilution 1:200). As this labeling is a transient labeling because the Cy3-Fluorophore is degraded over time, after fixation, permeabilization and DAPI staining quantification of cells that internalized the stained CD34-Cy3 receptor was done using Zeiss and Leica microscopes (Apotome, DM5000).

CD34/Aurora B stain

CD34 stain was performed as described above. After fixation, cells were permeabilized with 0.1% Triton X-100 and incubated 30 minutes at room temperature with Aurora B antibody (Abcam) at 1:100 dilution. Then, coverslips were washed and incubated with anti-rabbit FITC antibody? (Dianova, dilution 1:200) for 30 minutes at room temperature. Cells were covered after washing and counterstained with DAPI as described above. Cells were imaged using a Leica DM 5000 microscope. Cells in which Aurora B staining was located to the cytokinetic furrow were analyzed for the expression of CD34 marker.

Flow cytometry

Cells were harvested and resuspended in flow buffer (PBS, 1% BSA, 1 mmol/L EDTA). After three washes, and blockade of unspecific binding sites (2% BSA/PBS), cells were stained with primary antibodies. Measurements were done (80,000–500,000 live cells) on FACSCalibur and LSRII (BD Biosciences) flow cytometer (488 nm, 635 nm) equipped with four fluorescence photomultiplier filters.

qRT-PCR analysis

RNA isolation of treated or doxorubicin sorted cells was performed buffer according to the manufacturer's instructions (PeqGold; Roche). The removal of DNA from RNA was performed using DNAse (Life Technologies) according to the instructions. cDNA synthesis was performed using "RevertAid H Minus Strand cDNA Synthesis Kit" (Invitrogen) according to the instructions.

The detection of target gene mRNA levels was performed by qRT-PCR analysis with an ABI Prism 7000 Sequence Detection System (Applied Biosystems) and qPCR Maxima Mastermix (Fermentas) as previously described. Primer sequences can be obtained upon request.

Statistical analysis

Statistical analysis was performed with SigmaStat and GraphPad Prism 4 (2004). Additional and detailed methods are described in the Supplementary Information.

Results

mCXCL1 activates stem cell maintenance independent of proliferation

Tumor cells secrete inflammatory cytokines that affect cell signaling, self-renewal, and treatment resistance (6). To determine whether Cul3/p53 ko cells show a different secretory profile in comparison to Cul3 ko (control) cells, we performed a comparative ELISA-based Luminex assay on the supernatants of untreated cells. Cul3/p53 ko cells secreted significantly higher amounts of mCXCL1 (Fig. 1A). To determine the effect of increased mCXCL1 level, cells treated with mCXCL1 were analyzed by qRT-PCR analysis. An upregulation of self-renewal and stem cell maintenance-associated genes such as *sox2*, *bmi1*, and *nanog* (7) was detected (Fig. 1B). Expression of D site of albumin promoter binding protein (*dbp*), a liver-enriched transcriptional protein (8) was found to be downregulated, suggesting a dedifferentiated state (Fig. 1B). Furthermore, a flow-cytometry analysis of Cul3/p53 ko cells treated with mCXCL1 was performed and the expression of stem cell–related markers such as CD34, Sca-1, c-kit, and CD44 (4) was determined. We found that only the $CD34^+$ subpopulation accumulated significantly under the mCXCL1 treatment (Fig. 1C and D and Supplementary Fig. S1A). The $CD34^+$ cells expressed liver-associated markers (*albumin, dbp, hn-factors*) at lower levels

Published OnlineFirst August 3, 2016; DOI: 10.1158/0008-5472.CAN-15-3453

A

Factor	IL1ß	IL2	IL3	IL4	IL5	IL6	IL12	IL17	Eotaxin	G-CSF	GM-CSF	IFNg	CXCL1	MCP1	MIP1a	Rantes	TNFa
Cul3/p53ko	6.7	0.8	0.3	1.65	4.46	1.36	81.2	0.84	128.8	2.46	2.74	0.74	20755	2209	0.56	0.38	8.53
Cul3ko	6.7	0.8	0.29	1.51	7.89	1.75	190.5	0.77	130.8	2.38	2.0	0.61	5689	6786	0.63	1.22	6.96

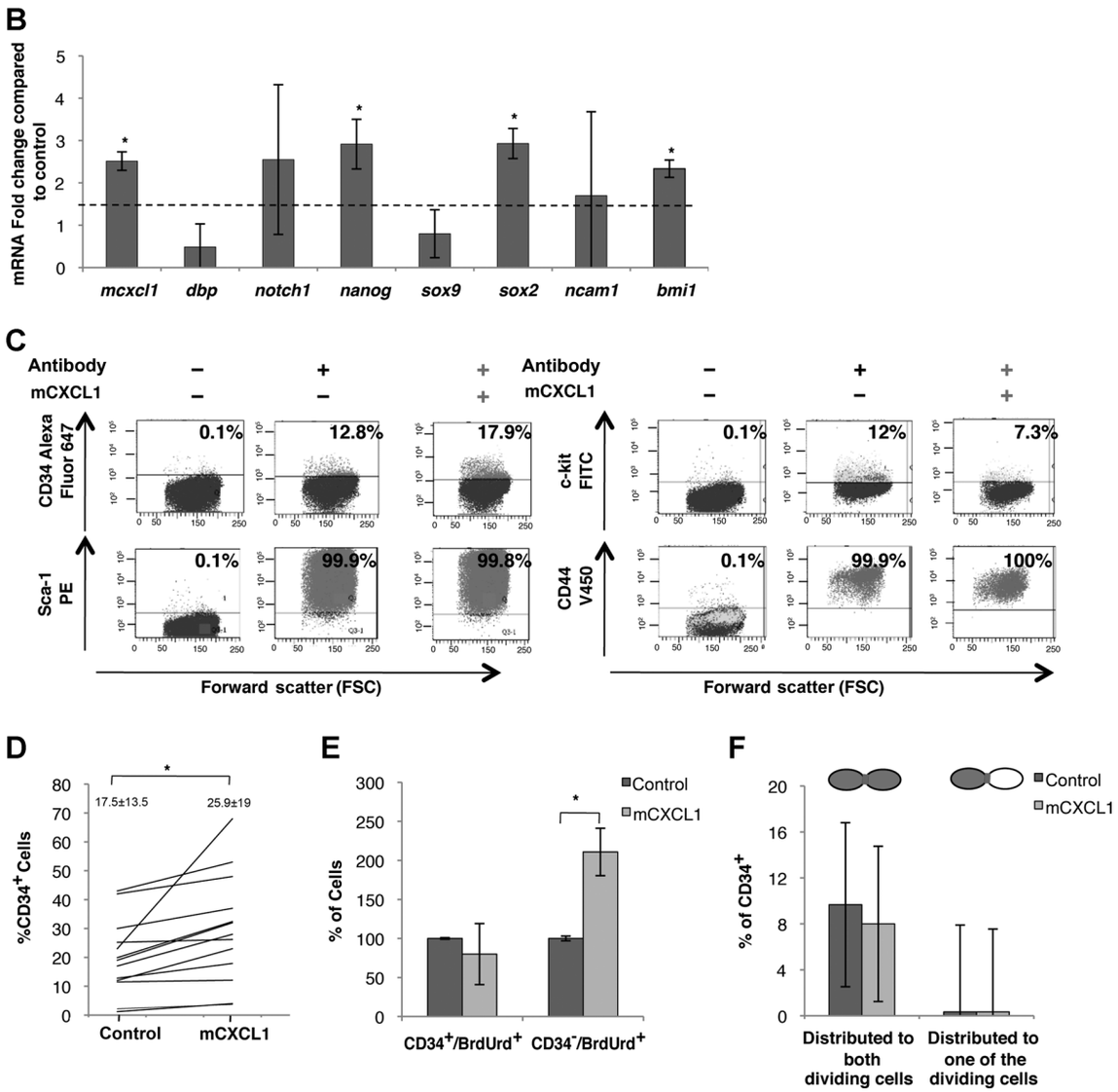

Figure 1.

mCXCL1 activates stem cell maintenance independent of proliferation. **A,** Luminex analysis of secreted factors (pg/mL) in asynchronously proliferating Cul3 and Cul3/p53 ko cells. mCXCL1 is indicated by the box. **B,** increased expression of stem cell–associated genes under mCXCL1 treatment. GAPDH was used as a housekeeping gene; ΔCp (fold change) values were calculated. Line shows 1.5-fold over control ($n = 2$). **C,** $CD34^+$ cells accumulate under mCXCL1 treatment. Flow cytometry analysis 48 hours after treatment with mCXCL8. A representative flow cytometry plot is shown (compare Supplementary Fig. S1A). **D,** summary of mCXCL1 treatments. A significant accumulation of premalignant $CD34^+$ progenitor cells under mCXCL1 treatment in Cul3/p53 ko cells ($n = 13$). **E,** cellular state–specific effects of mCXCL1. Proliferation analysis of Cul3/p53 ko cells under mCXCL1 treatment. Percentage of $CD34^-/BrdUrd^+$ and $CD34^+/BrdUrd^+$ cells in comparison to untreated cells ($n = 3$). **F,** symmetric distribution of CD34 in Cul3/p53 ko cells during cytokinesis upon mCXCL1 treatment of cells ($n = 3$). Scheme displays the analysis. Cytokinetic furrow and dividing cells were analyzed for CD34 expression ($CD34^+$ cells, dark gray; $CD34^+$, white).

Published OnlineFirst August 3, 2016; DOI: 10.1158/0008-5472.CAN-15-3453

than adult hepatocytes (Supplementary Fig. S1B, data represented as absolute Ct value normalized to its housekeeping GAPDH); and increased levels of hepatic stem cell markers such as CD44, CK14, CK18, CK19, as well as Sca-1 (Supplementary Fig. S1B; refs. 4, 9). We continued to examine the cellular state of $CD34^+$ cells in more detail by comparing $CD34^+$ to $CD34^-$ cells using qRT-PCR analysis: $CD34^-$ cells showed a decreased expression of *bmi1* and *oct4* as well an increased expression of albumin (Supplementary Fig. S1C). These results confirmed our previous studies showing that $CD34^-$ cells are more differentiated (2). Furthermore, not more than 1,000 $CD34^+$ cells sufficed to promote tumor growth with tendency toward decreased tumor incidence of 62.5% as compared to 75% in $CD34^-$ cells (Supplementary Fig. S1D).

Because mCXCL1 has been described as a mitogen for $CD133^+$ liver TICs (10), we further investigated the impact of mCXCL1 on the proliferation of $CD34^+$ cells. We measured bromdesoxyuridin (BrdUrd) uptake by flow cytometry. $CD34^-$ cells showed a significantly increased proliferation upon mCXCL1 stimulation (Fig. 1E). In contrast, BrdUrd uptake of $CD34^+$ cells remained unchanged. These results suggested that the accumulation of $CD34^+$ cells was not caused by increased proliferation.

The elevated numbers of $CD34^+$ cells could also be caused by a different distribution of CD34 on dividing cells. Based on this hypothesis, we would expect a depolarization of CD34. The dividing cell would produce two $CD34^+$ daughter cells upon mCXCL1 treatment instead of one $CD34^+$ and one $CD34^-$ daughter cell. Mitotic cells were identified by a combination of CD34 and Aurora B staining. We could not detect any changes in distribution of CD34 on dividing cells upon mCXCL1 treatment (Fig. 1F).

To summarize, mCXCL1 exerts opposing cellular functions on cells of different cellular states. Although $CD34^-$ TICs ($CD133^+$, $CK19^{+/}$; ref. 2) show increased proliferation $CD34^+$ cells accumulate in their more undifferentiated cellular stage under mCXCL1 treatment.

mCXCL1 blocks the differentiation of premalignant $CD34^+$ cells

We developed a single-cell approach based on an immunofluorescence cell-tracking assay to determine why $CD34^+$ cells accumulated under mCXCL1 treatment. This assay is based on the labeling of $CD34^+$ cells by the internalization of the Cy3 stained CD34 receptor and a second staining of the CD34 receptor using FITC-tagged antibodies (Fig. 2A and Supplementary Fig. S2A and S2B). The method, however, did not allow to determine the *de novo* synthesis of CD34 receptor. We quantified those cells showing intracellular red-fluorescence and determined re-exposure of the FITC-labeled CD34 receptor after 9 hours. Cells that showed an intracellular red fluorescent staining (1st CD34 stain) and also an extracellular FITC staining (2^{nd} CD34 stain) kept their stem cell phenotype. Single intracellular red stained cells (1st CD34 stain) differentiated. Quantification (Fig. 2B) revealed that mCXCL1 treatment led to a significant increase of undifferentiated cells of up to 16% (Fig. 2C).

Immunofluorescence staining was performed using anti-CK14 or anti-CK19 antibodies instead of anti-CD34 antibody in the second staining. CK14 is expressed on both $CD34^+$ and $CD34^-$ populations (2). CK19 is predominantly expressed on differentiating $CD34^-$ cells (2). A continuous expression of CK14 on $CD34^+$ cells and a significant decrease in $CD34^+/CK19^+$ cells upon mCXCL1 treatment was found (Fig. 2D and E).

Thus, we concluded that mCXCL1 promotes the maintenance of the cellular state of $CD34^+$ premalignant stem/progenitor cells by preventing their differentiation.

mTORC1 signaling mediates the maintenance of the premalignant stem/progenitor cells

To understand how maintenance of the premalignant stem/progenitor state of $CD34^+$ cells is induced by mCXCL1, the activation of signaling molecules downstream of the mCXCL1 receptors CXCR1 and CXCR2 was analyzed (11). Both receptors activate a broad array of intracellular signal transduction pathways including mTORC1, p38MAPK, PI3K-, and ERK signaling (12). Using a proteome profiler, an increased phosphorylation of AKT-2/-3 (13), CREB (14), JNK-3 (15), and p70-S6K (14) was found (Supplementary Fig. S3A). Because mTORC1 signaling represents a central signaling molecule within the signaling pathways of the identified kinases, the phosphorylation of the downstream located 4EBP-1 as an indicator of mTORC1 activity using Western blotting was determined (16). A slight but significant change in p4EBP-1 levels under mCXCL1 treatment was detected (Fig. 3A). The latter results could be confirmed by flow cytometry analysis showing that only a small subpopulation of proliferating Cul3/p53 ko cells are positive for p4EBP-1 (Fig. 3B), whereas adult hepatocytes do not show a phosphorylation of 4EBP-1 (Supplementary Fig. S3B).

As part of a functional analysis, the percentage of $CD34^+$ cells under mTORC1 blockade (Rad001) was detected and found to be significantly decreased in comparison to untreated cells (Fig. 3C). mTORC1 blockade was confirmed by Western blotting against phospho-S6 ribosomal protein (pS6RP) and 4EBP-1 (Fig. 3C). Propidium iodide stainings showed that the decrease of $CD34^+$ cells was not caused by increased cell death under Rad001 (Supplementary Fig. S3C). We also tracked single $CD34^+$ cells (compare to Fig. 2) and found a significant decrease of double positive (CD34Cy3/FITC) cells upon mTORC1 blockade (Fig. 3D). The differentiating effect could not be rescued by simultaneous treatment with mCXCL1, indicating that mCXCL1 and mTORC1 act in the same signaling cascade (Fig. 3E and Supplementary Fig. S3D).

Thus, we concluded that mCXCL1 mediates stem cell maintenance via mTORC1 activation.

To test if an association between mCXCL1 and stem cell maintenance could also be detected *in vivo*, a HCC mouse model was analyzed. In this mouse model, tumorigenesis is based on an increased expression of lymphotoxins (LTα and LTβ) and downstream target genes, mimicking the inflammatory signature of virus-infection induced (hepatitis B and hepatitis C) chronic liver inflammation (17). As the mice show an increased expression of mCXCL1 (17), we asked whether a correlation in the mTORC1 kinase activation in early hepatic progenitor cells of AlbLTαβ mice could be found. $CD34^+$ cells are located in the unaffected liver tissue in close proximity to the tumor or in the tumor tissue (Fig. 3F). Quantification of $CD34^+/pS6RP^+$ cells (Fig. 3G) indicated a significant increase in mTORC1 kinase activity in $CD34^+$.

Therefore, the inflammatory-driven HCC model supported our *in vitro* findings, demonstrating that increased mCXCL1 levels correlate with the activity of the mTORC1 complex in $CD34^+$ cells.

Published OnlineFirst August 3, 2016; DOI: 10.1158/0008-5472.CAN-15-3453

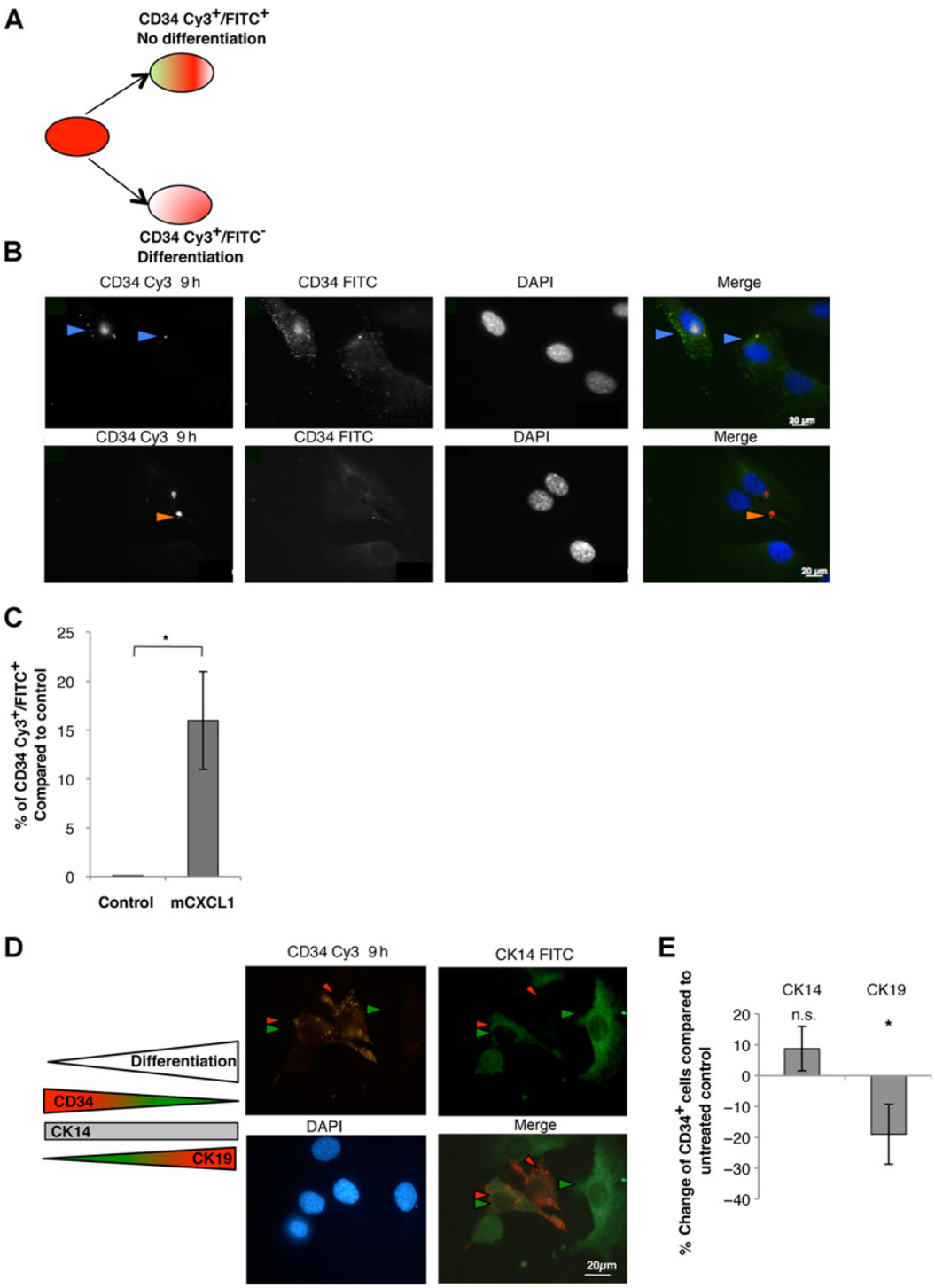

Figure 2.

mCXCL1 blocks the differentiation of premalignant CD34$^+$ cells. **A,** scheme of the differentiation assay for tracking of premalignant CD34$^+$ cells. **B,** a representative picture of Cul3/p53 ko cells under mCXCL1 treatment in the differentiation stain is shown. Blue arrows, double positive cell (not differentiated); orange arrows, single Cy3$^+$ cell (differentiated). **C,** inhibition of differentiation of CD34$^+$ premalignant stem/progenitors. Quantification of the differentiation assay in Cul3/p53 ko cells. Shown is the percentage difference to control cells ($n = 5$). **D,** schematic representation of marker regulation under differentiation of CD34$^+$ cells and representative image of Cul3/p53 double staining with CD34 (red) and CK14 (green). Arrowheads, a single CD34$^+$ cell (red); a single CK14$^+$ cell (green); a CD34$^+$/CK14$^+$ cell (red and green). **E,** Cul3/p53 ko cells treated with mCXCL1 were quantified for CD34/CK14 and CD34/CK19 positivity. Shown is the difference of double positive cells treated with mCXCL1 in comparison to untreated cells in percent (CK14, $n = 3$; CK19, $n = 4$).

Published OnlineFirst August 3, 2016; DOI: 10.1158/0008-5472.CAN-15-3453

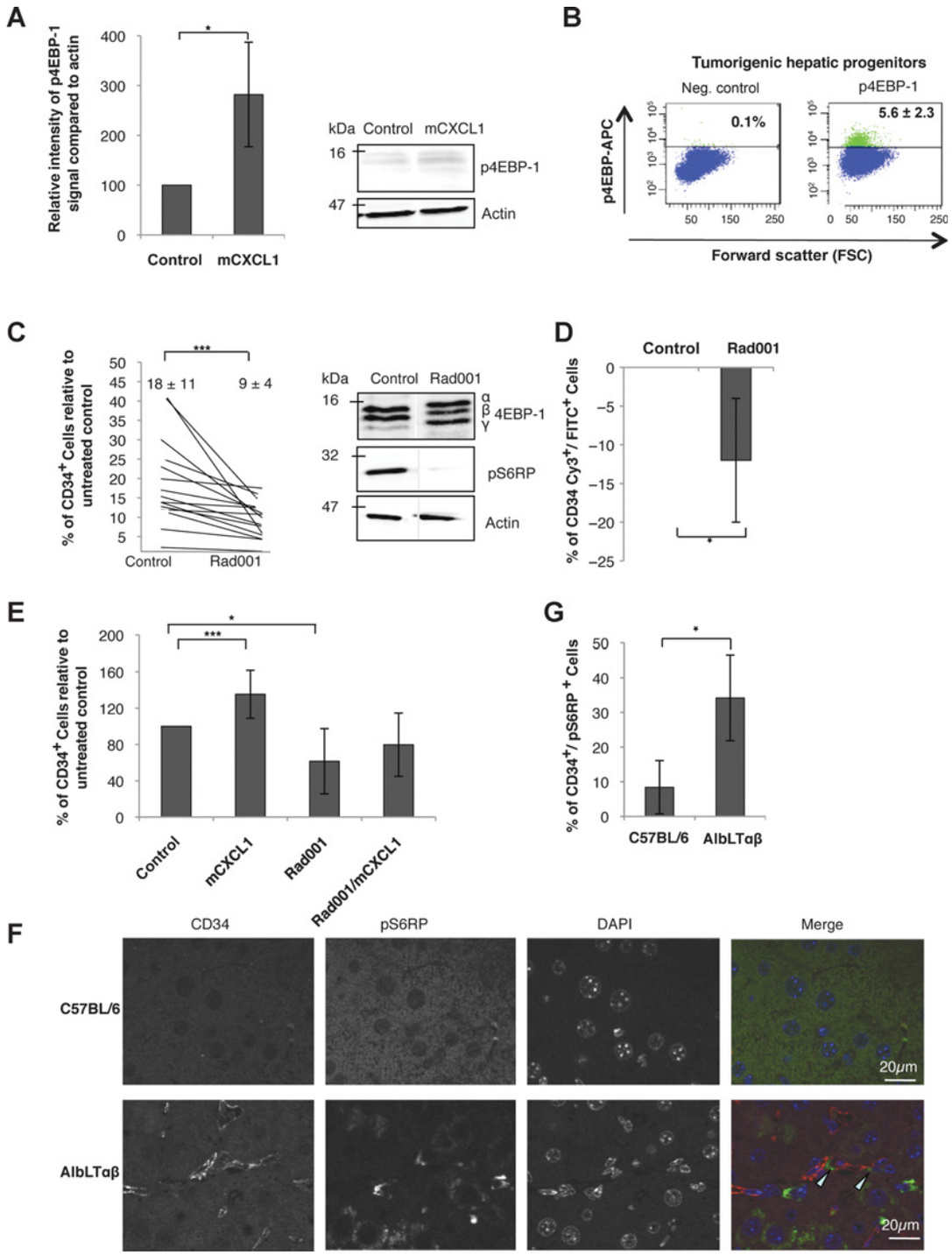

Figure 3.

mTORC1 signaling mediates the maintenance of the premalignant stem/progenitor cells. **A,** 4EBP-1 phosphorylation is increased under mCXCL1 treatment in Cul3/p53 ko cells. Western blots for p4EBP-1 were quantitated. Actin served as a control. **B,** a representative flow cytometry analysis of p4EBP-1 in Cul3/p53 ko ($n = 4$). **C,** decrease of $CD34^+$ Cul3/p53 ko cells under mTORC1 inhibition with Rad001 using flow cytometry ($n = 15$). Western blot analysis of 4EBP-1 and S6RP phosphorylation to monitor mTORC1 blockade. Actin served as a control. **D,** $CD34^+$ Cul3/p53 ko cells differentiate under mTORC1 inhibition ($n = 4$). Data were normalized to control. **E,** mTORC1 is located downstream of mCXCL1. Cul3/p53 ko cells were treated with mCXCL1, Rad001, or a combination of both, followed by flow cytometry for CD34 positive cells. Data were normalized to control (compare Supplementary Fig. S3D; $n = 9$). **F,** $CD34^+$ cells in the AlbLTab HCC mouse model are positive for pS6RP. Quantification of $CD34^+/pS6RP^+$ cells in AlbLTab transgenic livers (n: AlbLTab = 7, wt = 3). Quantified cells were located in the tumor tissue as well as next to the tumor tissue. **G,** staining of AlbLTab transgenic livers for CD34 (Cy3) and pS6RP (FITC) in comparison to wt livers. Representative pictures of these stainings are shown. Orange arrows, double positive cells.

Published OnlineFirst August 3, 2016; DOI: 10.1158/0008-5472.CAN-15-3453

mCXCL1 treatment and mTORC1 influence chemotherapy resistance by induction of quiescence

Next, the importance of the mCXCL1/mTORC1 cascade in chemotherapy resistance was analyzed. Tumorigenic hepatic progenitors were treated with the chemotherapeutic drug doxorubicin. Doxorubicin-treated cells displayed higher pS6RP levels than untreated cells (Fig. 4A). Flow cytometry of doxorubicin-treated cells revealed three different populations (doxorubicin negative, intermediate, and positive cells) identified by their specific PE (doxorubicin) intensity (Fig. 4B). Cells in these populations differed in their forward scatter (size) and sideward scatter (granularity; data not shown). We sorted three doxorubicin populations and measured their cell size. Doxorubicin negative (PE^-) cells showed a significantly smaller cell size (Fig. 4C), which could be indicative for an undifferentiated cellular state. Flow cytometry analysis demonstrated a significant increase of $CD34^+$/p4EBP-1^+ population among doxorubicin intermediate and negative cells (Fig. 4D), which correlated with an overall accumulation of p4EBP-1 [doxorubicin negative: 3.1% ± 1.6%; doxorubicin intermediate: 26% ± 8% ($n = 4$)].

The interference with the mCXCL1–mTORC1 pathway by activating with mCXCL1 or by blocking it, with the mTORC1 inhibitor Rad001, significantly increased (mCXCL1) or decreased (Rad001) the number of doxorubicin-resistant cells as measured by flow cytometry (Fig. 4E and Supplementary Fig. S4A). In addition, mCXCL1 treatment significantly increased the percentage of $CD34^+$ doxorubicin negative cells (Fig. 4F).

Expression analysis in three enriched doxorubicin populations revealed an increase of mCXCL1 expression that correlated with an enhanced expression of *nanog*, *bmi1*, and *sox2* (Fig. 4G, also compare Fig. 1B). Furthermore, we performed cell-cycle analysis using DAPI and found that doxorubicin-escaping cells accumulated in G_1-phase of the cell cycle (Fig. 4H and Supplementary Fig. S4B).

In concordance with our previous data we concluded that chemotherapy resistance is mediated by the mCXCL1–mTORC1 axis, a phenotype that is associated with a nonproliferate cellular state.

hHCC displays the same resistance phenotype

To test whether these findings might be of clinical relevance, four different hHCC cell lines with different genetic background were analyzed. Expression analysis of cells treated with doxorubicin showed an upregulation of hCXCL8, the human homolog of mCXCL1 (Fig. 5A). Furthermore, doxorubicin negative and intermediate cells also accumulated in G_1 phase (Fig. 5B) of the cell cycle. p4EBP-1 accumulation could also be detected in the doxorubicin negative and intermediate population in three out of four cell lines (Fig. 5C and Supplementary Fig. S5A and S5B).

Finally, mTORC1 was blocked and the percentage of doxorubicin negative cells was analyzed. Blockade of mTORC1 signaling under doxorubicin treatment led to decreased numbers of escaping cells, however, not in Huh6 cells (Fig. 5D and Supplementary Fig. S5B). Interestingly, the decrease in resistant cells correlated with an increased autofluorescence of doxorubicin (Fig. 5E) indicative for a reduced ability to escape the chemotherapeutic treatment.

Induction of differentiation by mTORC1 inhibition as a beneficial therapeutic approach

In human HCC, the accumulation of stem cell markers and TIC markers such as CD44, CD90, and CD133 correlate with the de-differentiation of the tumor (18), of which CD90 and CD44 accumulated under doxorubicin treatment in Huh7 cells (Supplementary Fig. S6A). CD133 and CD44 have been also described as hepatic (19) and precancerous markers (20).

Interestingly, the percentage of $CD44^+$ cells in Huh7 cells correlated with the increased hCXCL8 levels in comparison to HepG2 cells (Supplementary Fig. S6B and S6C). They induced the observed phenotype (Supplementary Fig. S6D). Upon doxorubicin treatment and mTORC1 blockade, mainly $CD44^+$ cells showed a significant decrease (Fig. 6A and B and Supplementary Fig. S6E).

To underpin the induction of differentiation as a possible therapeutic approach, we hypothesized that a combinational approach is more efficient than a chemotherapeutic treatment alone. Thus, Huh7 tumors were established and treated using doxorubicin, Rad001, or a combination of both. Single treatment slowed down the tumor growth. The combination therapy significantly reduced tumor growth (Fig. 6C). Comparing hematoxylin and eosin stainings of control or single and combinational treated tumors revealed increase in necrotic tissue (Fig. 6D). Therefore, Western blotting was performed to compare CD44 and AFP in untreated to treated samples and a correlation of these markers with p4EBP-1 intensity was found (Fig. 6E, compare also Fig. 6D).

We concluded that the mCXCL1/hCXCL8–mTORC1 signaling pathway mediates chemotherapy resistance by activation of stem cell maintenance correlated with nonproliferative cellular state. This approach is of translational importance, as mTORC1 blockade under chemotherapy treatment significantly reduces the percentage of resistant cells and is likely to improve the survival of cancer patients.

Discussion

HCC is characterized by the presence of TICs, whose origin is still under debate (5, 21, 22). Here, we elucidated a new resistance mechanism specific to premalignant hepatic cells. We found a significant increase in mCXCL1 secretion in Cul3/p53 ko cells in comparison to their nontumorigenic counterpart (Cul3 ko cells). mCXCL1 is the mouse homolog of hCXCL8 (23). Increased hCXCL8 levels correlate with poor prognosis (24), increased angiogenesis, growth, and self-renewal of TICs (10). In our work, we underpin the important function of hCXCL8 and its proposed use as prognostic factor. The establishment of a single cell tracking assay, a method that does not address de-differentiation, allowed us to determine that mCXCL1/hCXCL8 activates cellular quiescence and blocks the differentiation in dependence of the mTORC1 kinase. Other chemokines whose pathways are cross-linked to mTORC1 (25), might also support the here described resistance phenotype. Our data point to a parallel mechanism to the recently published G_{Alert} phase of adult stem cells (26). Upon cellular stress such as an exposure to chemotherapy, cells enter a G_{Alert} phase and maintain stemness by well-known pluripotency factors (7, 27, 28).

Interestingly, mTORC1 blockade did not only deplete surviving cells but significantly reduced the percentage of doxorubicin

Published OnlineFirst August 3, 2016; DOI: 10.1158/0008-5472.CAN-15-3453

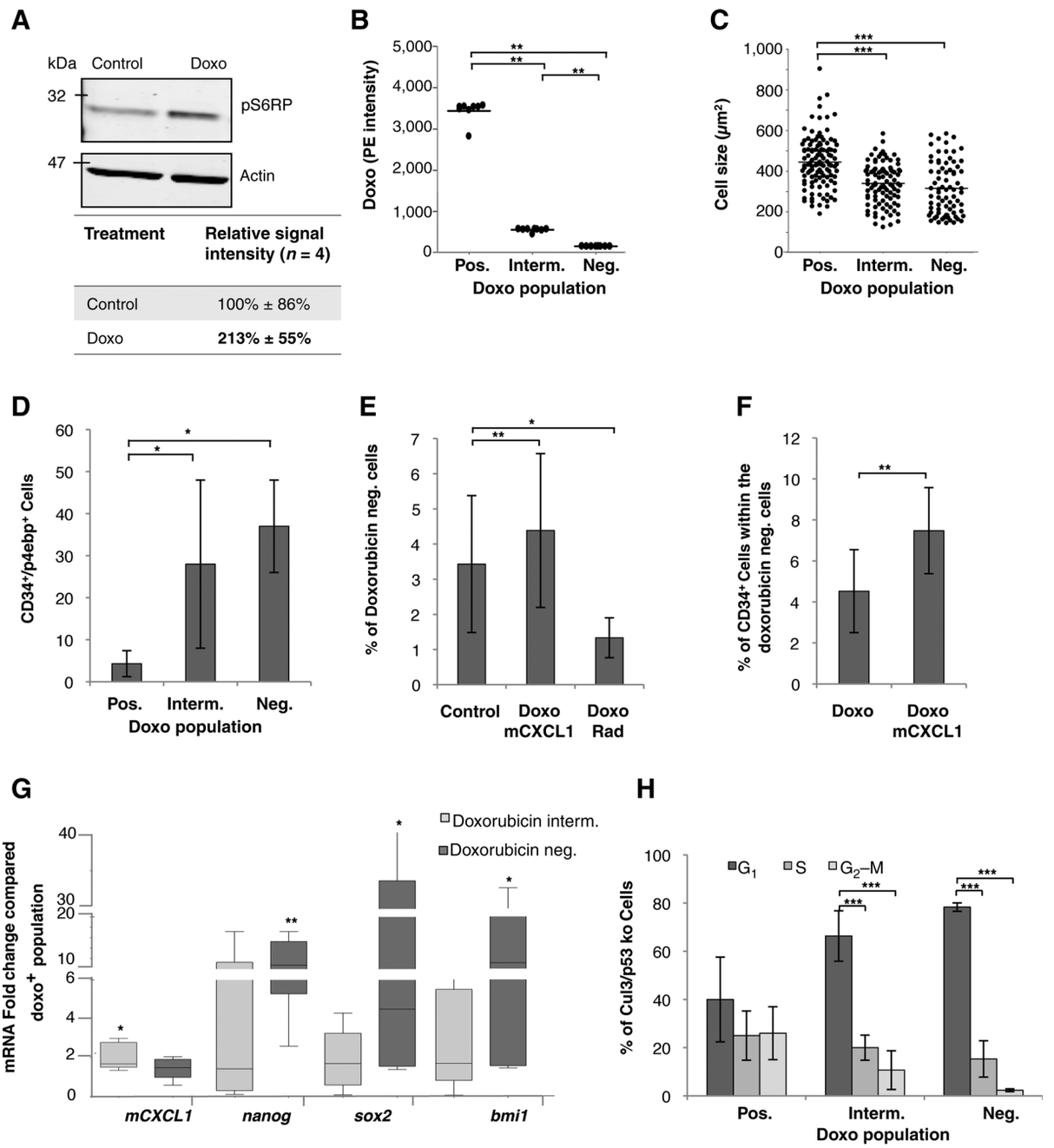

Figure 4.

mCXCL1 treatment and mTORC1 influence chemotherapy resistance by induction of quiescence. **A,** mTORC1 is activated under doxorubicin treatment. Western blot analysis of Cul3/p53 ko cells for pS6RP under doxorubicin treatment (Doxo) in comparison to untreated control cells. Actin was used as a loading control ($n = 4$). **B,** Cul3/p53 ko cells were treated with doxorubicin. Three populations of cells could be distinguished. **C,** measurement of cell size of sorted doxorubicin populations using Axio Vision Software. Graph depicts the cell size as area in μm^2 ($n = 2$, 100 cells/experiment). Mann–Whitney *U* test was used to calculate significances. **D,** $CD34^+/p4EBP\text{-}1^+$ cells escape doxorubicin treatment. Doxorubicin-treated Cul3/p53 ko cells stained for CD34 and p4EBP-1 were analyzed by flow cytometry ($n = 5$). **E,** mCXCL1 treatment and mTORC1 blockade significantly influenced resistance of tumorigenic hepatic progenitors. **F,** increase of $CD34^+$ doxorubicin negative cells under mCXCL1 treatment determined by flow cytometry (same experimental setting as in **E**; $n = 4$). **G,** expression analysis of stem cell–associated markers and mCXCL1 in doxorubicin intermediate and negative population in Cul3/p53 ko cells compared with the doxorubicin positive population. **H,** doxorubicin escaping cells accumulate in G_1. Cell-cycle analysis of doxorubicin-treated Cul3/p53 ko cells (compare with Supplementary Fig. S4A).

Published OnlineFirst August 3, 2016; DOI: 10.1158/0008-5472.CAN-15-3453

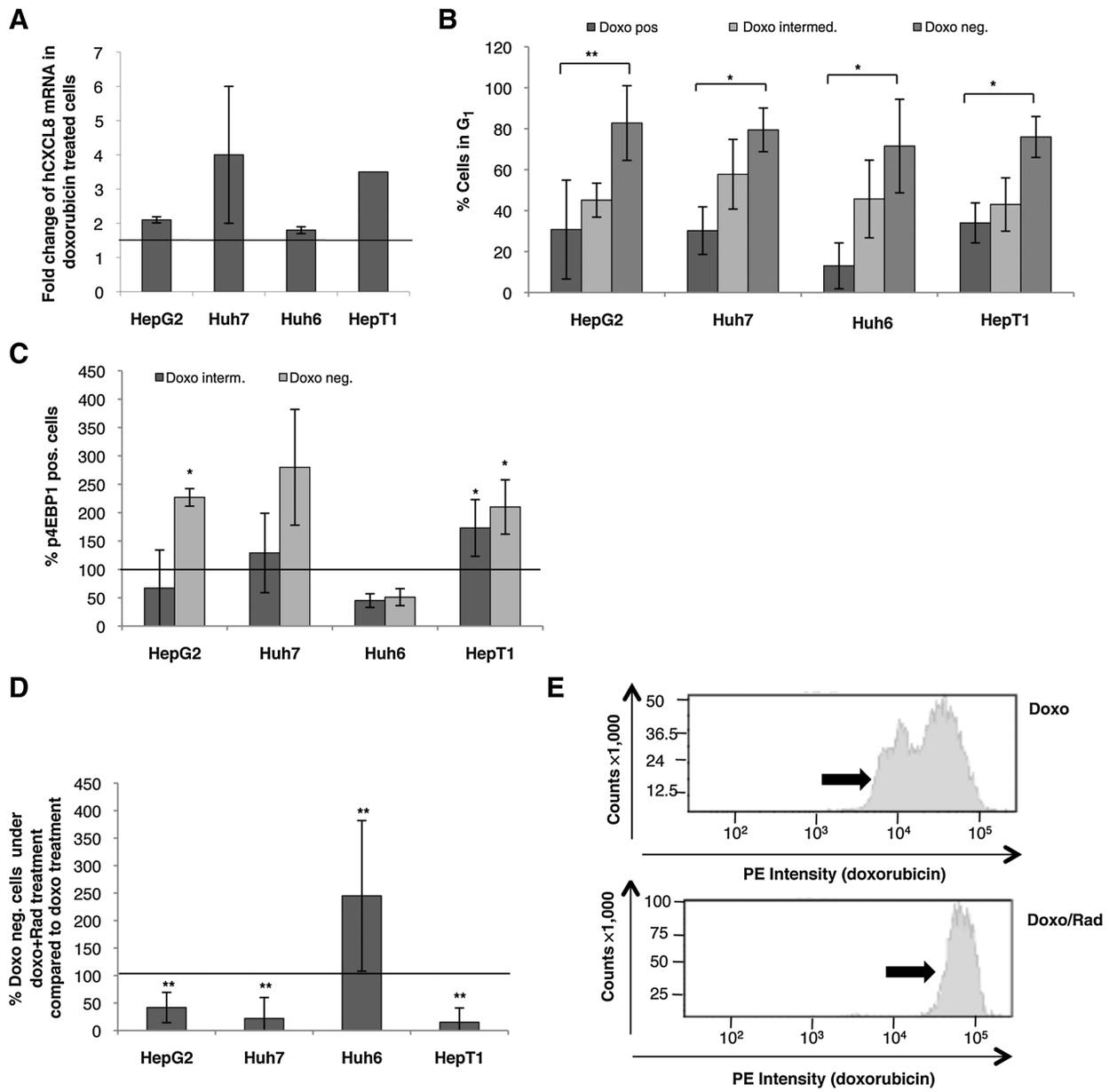

Figure 5.

hHCC cell lines display the same resistance phenotype. **A,** hCXCL8 expression is increased upon doxorubicin treatment. Cells were treated with 2 μg/mL doxorubicin and harvested 48 hours later for expression analysis. GAPDH and actin served as a control; fold change is shown. **B,** accumulation of cells in G_1 phase upon doxorubicin escape. Cell-cycle analysis in four HCC cell lines after under 48 hours of doxorubicin treatment (2 μg/mL doxorubicin). **C,** p4EBP-1 positivity in doxorubicin-treated cells. p4EBP-1 positivity was measured by flow cytometry. Relative data are shown ($n = 3$). **D,** significant decrease of doxorubicin negative cells under mTORC1 blockade by Rad001 in hHCC cells, measured by flow cytometry. **E,** increased doxorubicin autofluorescence upon Rad001 treatment. A representative flow cytometry analysis is shown for HepG2 cells. Doxorubicin autofluorescence was measured in the PE-channel. Upon treatment with Rad001, autofluorescence increases. This is indicative of decreased ability to escape the treatment. The increase of autofluorescence correlates with decreased percentage of surviving cells.

intermediate cells, indicating that mTORC1 activity is the most important to achieve resistance.

Our study implies a hierarchical order of TICs in hHCC. However, detailed studies of markers and characteristics of TICs and their relation have not been performed.

The importance of our study is underlined by the finding that mTORC1 activity has recently been shown to also mediate sorafenib resistance (29). Another study showed that increased expression of pluripotency factors is also induced by cyclophosphamide, a drug that blocks angiogenesis (30).

Published OnlineFirst August 3, 2016; DOI: 10.1158/0008-5472.CAN-15-3453

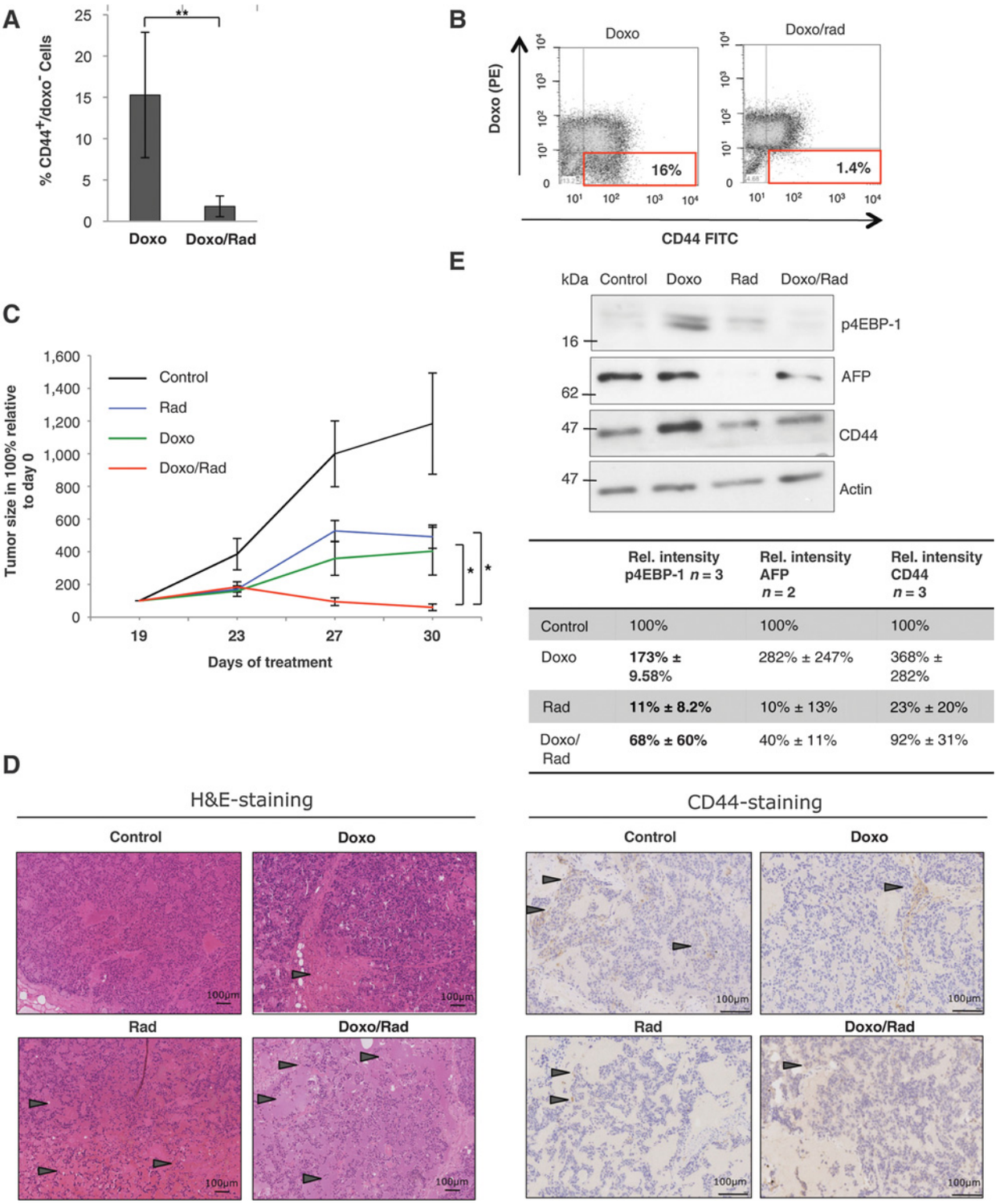

	Rel. intensity p4EBP-1 $n = 3$	Rel. intensity AFP $n = 2$	Rel. intensity CD44 $n = 3$
Control	100%	100%	100%
Doxo	**173% ± 9.58%**	282% ± 247%	368% ± 282%
Rad	**11% ± 8.2%**	10% ± 13%	23% ± 20%
Doxo/Rad	**68% ± 60%**	40% ± 11%	92% ± 31%

Figure 6.

Induction of differentiation by mTORC1 inhibition as a beneficial therapeutic approach. **A,** mTORC1 blockade decreases $CD44^+$ doxorubicin-negative Huh7 cells. Quantification of $CD44^+$/doxorubicin$^-$ cells ($n = 5$). **B,** representative flow cytometry of CD44-stained Huh7 cells treated with doxorubicin or doxorubicin/Rad001. **C,** tumor growth is reduced by a combinational therapy. Xenotransplants of Huh7 cells in NMRInu/nun mice treated with doxorubicin, Rad001, or a combination. The tumor volume at day 0 was set to 100%. Untreated tumors ($n = 10$) to doxorubicin/Rad001-treated tumors ($n = 9$). Doxorubicin-treated ($n = 7$) to doxorubicin/Rad001–treated tumors. **D,** hematoxylin and eosin (H&E; ×20) and CD44 (×40) stainings of tumor samples at day 30 after the treatments. Arrowheads, necrotic tissue areas. **E,** Western blot quantification of stem cell markers in xenografts after explantation of tumors.

Published OnlineFirst August 3, 2016; DOI: 10.1158/0008-5472.CAN-15-3453

These studies point to more general resistance phenotype and are in line with our data.

Although further studies have to be performed to confirm resistance mechanisms using different mouse models, the results of our study underline the importance of combinational therapeutic approaches.

Disclosure of Potential Conflicts of Interest

No potential conflicts of interest were disclosed.

Authors' Contributions

Conception and design: B. Wolf, U. Kossatz-Boehlert

Development of methodology: B. Wolf, S. Hauser, U. Kossatz-Boehlert

Acquisition of data (provided animals, acquired and managed patients, provided facilities, etc.): B. Wolf, K. Krieg, C. Falk, H. Keppeler, T. Biedermann, E. Schmid, S. Warmann, J. Fuchs, D. Thiele, M. Nieser, L. Schöls, S. Hauser, M. Ringelhahn, U. Kossatz-Boehlert

Analysis and interpretation of data (e.g., statistical analysis, biostatistics, computational analysis): B. Wolf, M. Avci-Adali, M. Heikenwalder, U. Kossatz-Boehlert

Writing, review, and/or revision of the manuscript: B. Wolf, K. Breuhahn, T. Biedermann, S. Warmann, M. Nieser, M. Avci-Adali, L. Schöls, T. Yevsa, M. Heikenwalder, U. Kossatz-Boehlert

Administrative, technical, or material support (i.e., reporting or organizing data, constructing databases): H. Keppeler, T. Biedermann, E. Schmid, S. Warmann, J. Fuchs, S. Vetter, D. Thiele, M. Nieser, M. Avci-Adali, Yu. Skokowa, L. Schöls, M. Heikenwalder, U. Kossatz-Boehlert

Study supervision: J. Fuchs, U. Kossatz-Boehlert

Acknowledgments

We thank N. Malek for critically reading the manuscript and discussing the data. The authors thank M. Schwab for support, helpful discussion, and critically reading the manuscript. We thank Cornelia Grimmel from the Core Facility of the Interdisciplinary Center for Clinical Research of the University Hospital of Tübingen.

Grant Support

This work was supported by a grant from the German Research Foundation (KO 3999/1-2 to U. Kossatz-Boehlert). Heiknwälder Mathias was supported by the ERC starting Grant "LiverCancerMech," an ERC Consolidator Grant "HepatoMetaboPath," the Stiftung für "Biomedizinische Forschung" (Hofschneider foundation), and the Preclinical Comprehensive Cancer Center (PCCC) Helmholtz Alliance. T. Yevsa is funded by the German Research Foundation (DFG, YE 151/2-1).

The costs of publication of this article were defrayed in part by the payment of page charges. This article must therefore be hereby marked *advertisement* in accordance with 18 U.S.C. Section 1734 solely to indicate this fact.

Received December 18, 2015; revised May 10, 2016; accepted June 27, 2016; published OnlineFirst August 3, 2016.

References

1. Jemal A, Bray F, Center MM, Ferlay J, Ward E, Forman D. Global cancer statistics. CA Cancer J Clin 2011;61:69–90.
2. Kossatz U, Breuhahn K, Wolf B, Hardtke-Wolenski M, Wilkens L, Steinemann D, et al. The cyclin E regulator cullin 3 prevents mouse hepatic progenitor cells from becoming tumor-initiating cells. J Clin Invest 2010;120:3820–33.
3. Singer JD, Gurian-West M, Clurman B, Roberts JM. Cullin-3 targets cyclin E for ubiquitination and controls *S* phase in mammalian cells. Genes Dev 1999;13:2375–87.
4. Mishra L, Banker T, Murray J, Byers S, Thenappan A, He AR, et al. Liver stem cells and hepatocellular carcinoma. Hepatology 2009;49:318–29.
5. Yamashita T, Wang XW. Cancer stem cells in the development of liver cancer. J Clin Invest 2013;123:1911–8.
6. Dranoff G. Cytokines in cancer pathogenesis and cancer therapy. Nat Rev Cancer 2004;4:11–22.
7. Herreros-Villanueva M, Zhang JS, Koenig A, Abel EV, Smyrk TC, Bamlet WR, et al. SOX2 promotes dedifferentiation and imparts stem cell-like features to pancreatic cancer cells. Oncogenesis 2013;2:e61.
8. Schrem H, Klempnauer J, Borlak J. Liver-enriched transcription factors in liver function and development. Part II: the C/EBPs and D site-binding protein in cell cycle control, carcinogenesis, circadian gene regulation, liver regeneration, apoptosis, and liver-specific gene regulation. Pharmacol Rev 2004;56:291–330.
9. Nagy P, Bisgaard HC, Thorgeirsson SS. Expression of hepatic transcription factors during liver development and oval cell differentiation. J Cell Biol 1994;126:223–33.
10. Tang KH, Ma S, Lee TK, Chan YP, Kwan PS, Tong CM, et al. CD133(+) liver tumor-initiating cells promote tumor angiogenesis, growth, and self-renewal through neurotensin/interleukin-8/CXCL1 signaling. Hepatology 2012;55:807–20.
11. Holmes WE, Lee J, Kuang WJ, Rice GC, Wood WI. Structure and functional expression of a human interleukin-8 receptor. Science 1991;253:1278–80.
12. Waugh DJ, Wilson C. The interleukin-8 pathway in cancer. Clin Cancer Res 2008;14:6735–41.
13. Manning BD, Cantley LC. AKT/PKB signaling: navigating downstream. Cell 2007;129:1261–74.
14. Liu Z, Chen X, Wang Y, Peng H, Jing Y, Zhang H. PDK4 protein promotes tumorigenesis through activation of cAMP-response element-binding protein (CREB)-Ras homolog enriched in brain (RHEB)-mTORC1 signaling cascade. J Biol Chem 2014;289:29739–49.
15. Kwak D, Choi S, Jeong H, Jang JH, Lee Y, Jeon H, et al. Osmotic stress regulates mammalian target of rapamycin (mTOR) complex 1 via c-Jun *N*-terminal kinase (JNK)-mediated raptor protein phosphorylation. J Biol Chem 2012;287:18398–407.
16. Laplante M, Sabatini DM. mTOR signaling in growth control and disease. Cell 2012;149:274–93.
17. Haybaeck J, Zeller N, Wolf MJ, Weber A, Wagner U, Kurrer MO, et al. A lymphotoxin-driven pathway to hepatocellular carcinoma. Cancer Cell 2009;16:295–308.
18. Liu R, Shen Y, Nan K, Mi B, Wu T, Guo J, et al. Association between expression of cancer stem cell markers and poor differentiation of hepatocellular carcinoma: a meta-analysis (PRISMA). Medicine 2015;94:e1306.
19. Chen Q, Khoury M, Limmon G, Choolani M, Chan JK, Chen J. Human fetal hepatic progenitor cells are distinct from, but closely related to, hematopoietic stem/progenitor cells. Stem Cells 31:1160–9.
20. Zheng YW, Tsuchida T, Shimao T, Li B, Takebe T, Zhang RR, et al. The CD133+CD44+ precancerous subpopulation of oval cells is a therapeutic target for hepatocellular carcinoma. Stem Cells Dev 2013;23:2237–49.
21. Lee JS, Heo J, Libbrecht L, Chu IS, Kaposi-Novak P, Calvisi DF, et al. A novel prognostic subtype of human hepatocellular carcinoma derived from hepatic progenitor cells. Nat Med 2006;12:410–6.
22. Dean M, Fojo T, Bates S. Tumor stem cells and drug resistance. Nat Rev Cancer 2005;5:275–84.
23. Richmond A, Balentien E, Thomas HG, Flaggs G, Barton DE, Spiess J, et al. Molecular characterization and chromosomal mapping of melanoma growth stimulatory activity, a growth factor structurally related to β-thromboglobulin. EMBO J 1988;7:2025–33.
24. Li XP, Yang XY, Biskup E, Zhou J, Li HL, Wu YF, et al. Co-expression of CXCL8 and HIF-1α is associated with metastasis and poor prognosis in hepatocellular carcinoma. Oncotarget 2015;6:22880–9.
25. Saleiro D, Platanias LC. Intersection of mTOR and STAT signaling in immunity. Trends Immunol 2015;36:21–9.
26. Rodgers JT, King KY, Brett JO, Cromie MJ, Charville GW, Maguire KK, et al. mTORC1 controls the adaptive transition of quiescent stem cells from G0 to G(Alert). Nature 2014;510:393–6.
27. Zhang R, Xu LB, Yue XJ, Yu XH, Wang J, Liu C. Bmi1 gene silencing inhibits the proliferation and invasiveness of human hepatocellular carcinoma

cells and increases their sensitivity to 5-fluorouracil. Oncol Rep 2013;29: 967–74.
28. Silva J, Nichols J, Theunissen TW, Guo G, van Oosten AL, Barrandon O, et al. Nanog is the gateway to the pluripotent ground state. Cell 2009;138:722–37.
29. Masuda M, Chen WY, Miyanaga A, Nakamura Y, Kawasaki K, Sakuma T, et al. Alternative mammalian target of rapamycin (mTOR) signal activation in sorafenib-resistant hepatocellular carcinoma cells revealed by array-based pathway profiling. Mol Cell Proteomics 2014;13: 1429–38.
30. Marfels C, Hoehn M, Wagner E, Gunther M. Characterization of in vivo chemoresistant human hepatocellular carcinoma cells with transendothelial differentiation capacities. BMC Cancer 2013; 13:176.

Cancer Research
The Journal of Cancer Research (1916–1930) | The American Journal of Cancer (1931–1940)

AACR American Association for Cancer Research

Inducing Differentiation of Premalignant Hepatic Cells as a Novel Therapeutic Strategy in Hepatocarcinoma

Benita Wolf, Kathrin Krieg, Christine Falk, et al.

Cancer Res 2016;76:5550-5561. Published OnlineFirst August 3, 2016.